Cellular Physiology and Biochemistry

Cell Physiol Biochem 2014;33:1789-1801
DOI: 10.1159/000362958
Published online: May 27, 2014
Accepted: April 25, 2014

1421-9778/14/0336-1789$39.50/0

Original Paper

The Predominant Pathway of Apoptosis in THP-1 Macrophage-Derived Foam Cells Induced by 5-Aminolevulinic Acid-Mediated Sonodynamic Therapy is the Mitochondria-Caspase Pathway Despite the Participation of Endoplasmic Reticulum Stress

Huan Wang[a] Yang Yang[a] Haibo Chen[a] Juhua Dan[b] Jiali Cheng[a] Shuyuan Guo[a] Xin Sun[a] Wei Wang[a] Yiwei Ai[a] Shuchang Li[a] Zhixin Li[a] Li Peng[a] Zhen Tian[b] Liming Yang[b] Jichao Wu[b] Xin Zhong[b] Qi Zhou[c] Peng Wang[c] Zhiguo Zhang[c] Wenwu Cao[c,d] Ye Tian[a,b]

[a]Division of Cardiology, the First Affiliated Hospital, Cardiovascular Institute, Harbin Medical University, [b]Department of Pathophysiology, the State-Province Key Laboratories of Biomedicine-Pharmaceutics of China, Key Laboratory of Cardiovascular Research, Ministry of Education, [c]Laboratory of Photo- and Sono-theranostic Technologies and Condensed Matter Science and Technology Institute, Harbin Institute of Technology, Harbin, China, [d]Materials Research Institute, The Pennsylvania State University, University Park, Pennsylvania, USA

Key Words
Foam cell • Apoptosis • 5-aminolevulinic acid • Sonodynamic therapy • Mitochondria pathway • ER stress • Atherosclerosis • Reactive oxygen species

Abstract
Background: In advanced atherosclerosis, chronic endoplasmic reticulum (ER) stress induces foam cells apoptosis and generates inflammatory reactions. ***Methods:*** THP-1 macrophage-derived foam cells (FC) were incubated with 1 mM 5-aminolevulinic acid (ALA). After ALA mediated sonodynamic therapy (ALA-SDT), apoptosis of FC was assayed by Annexin V-PI staining. Intracellular reactive oxygen species (ROS) and mitochondrial membrane potential were detected by staining with CellROX® Green Reagent and jc-1. Pretreatment of FC with N-acetylcysteine (NAC), Z-VAD-FMK or 4-phenylbutyrate (4-PBA), mitochondria apoptotic pathway associated proteins and C/EBP-homologous (CHOP) expressions were assayed by wertern blotting. ***Results:*** Burst of apoptosis of FC was observed at 5-hour after ALA-SDT with 6-hour incubation of ALA and 0.4 W/cm^2 ultrasound. After ALA-SDT, intracellular ROS level increased and mitochondrial membrane potential collapsed. Translocations of cytochrome

Ye Tian

Division of Cardiology, the First Affiliated Hospital, Harbin Medical University, 23 Youzheng Street, Harbin 150001, (China)
Tel/Fax +86-451-8555-5943, E-Mail yetian@ems.hrbmu.edu.cn

c from mitochondria into cytosol and Bax from cytosol into mitochondria, cleaved caspase 9, cleaved caspase 3, upregulation of CHOP, as well as downregulation of Bcl-2 after ALA-SDT were detected, which could be suppressed by NAC. Activation of mitochondria-caspase pathway could not be inhibited by 4-PBA. Cleaved caspase 9 and caspase 3 as well as apoptosis induced by ALA-SDT could be inhibited by Z-VAD-FMK. ***Conclusion:*** The mitochondria-caspase pathway is predominant in the apoptosis of FC induced by ALA-SDT though ER stress participates in.

Introduction

Atherosclerosis remains to be the leading cause of morbidity and mortality in industrialised countries [1, 2]. The presence of cholesterol-rich foam cells is a hallmark of an atherosclerotic lesion [3]. In all stages of atherosclerotic lesions, foam cells secret inflammatory cytokines and other molecules that contribute to lesion progression [4]. In early lesions, induction of foam cell apoptosis coupled with effective phagocytosis can retard lesion progression. While in advanced lesions, foam cells undergo endoplasmic reticulum (ER) stress induced by excessive free cholesterol accumulation [5-7]. Apoptotic foam cells triggered by chronic ER stress are a source of pro-inflammatory cytokines and proteases, which cannot be coupled with proper efferocytosis because the phagocytes nearby the apoptotic cells are vulnerable to death [5-7]. In this setting, the death mode of apoptotic cells shifts to secondary necrosis expanding the necrotic core and ultimately precipitating in plaque rupture [5]. Therefore, a method that could temporarily induce the burst of apoptosis among advanced lesion foam cells (including surrounding unhealthy phagocytes), rather than chronic ER stress, might facilitate homeostasis restoration and inflammation resolution within the advanced plaque.

Sonodynamic therapy (SDT), which was developed by Umemura et al. in 1989 for cancer treatment, is a non-thermal synergistic method utilising low-intensity ultrasound and sonosensitisers [8]. Sonosensitisers preferentially accumulate in tumour cells and macrophages because of the reduced ferrochelatase activity and enhanced porphobilinogen deaminase activity, and they are activated by ultrasound in the targeted area and generate reactive oxygen species (ROS), thus resulting in the killing of cells [9-12]. The most commonly used sonosensitisers, namely hemotoporphyrin (Hp), and their derivatives, such as protoporphyrin IX (PpIX), are rapidly excreted from the body within a few hours with little residual cellular toxicity [13]. The biological precursor of PpIX in the haeme biosynthesis pathway is 5-aminolevulinic acid (ALA), and PpIX derived from ALA mainly accumulates in mitochondria [14-16]. Because of the limited diffusion distance and nanosecond lifetime of ROS, the sub-cellular localisation of the sonosensitiser is of particular importance because it determines the initial damaged organelles [14, 17-19]. Mitochondria are essential in determining the point-of-no-return of the apoptotic process [20, 21]. The mitochondrial apoptotic pathway is considered the preferred death mode in vertebrate cells due to the anti-inflammatory reactions that follow [22, 23].

The effects of ALA-mediated sonodynamic therapy (ALA-SDT) on tumour cells have been extensively investigated in the past decade. Some studies have elucidated that ALA-SDT can induce the mitochondrial apoptotic pathway of tumour cells, but it is unclear if ER stress is also activated and contributes to the mitochondrial apoptotic pathway [15, 16]. There are also a few reports on the effects of ALA-SDT on macrophages and foam cells. Previously, we reported that ALA-SDT is capable of inducing apoptosis in THP-1 macrophages [24]. Nevertheless, nearly all of the macrophages in advanced plaques are transformed into foam cells, and the pharmacokinetics of ALA and ultrasonic parameters for the induction of apoptosis in foam cells may differ from normal macrophages. In this study, we investigated the sub-cellular location of the sonosensitiser, ALA-PpIX, in THP-1 macrophage-derived foam cells (FCs) as well as the activation of the mitochondrial apoptotic pathway and induction of ER stress by ALA-SDT.

Materials and Methods

Cell culture and foam cell formation

Human THP-1 cells (American Type Culture Collection [ATCC], Manassas, VA, USA) were seeded in 35 mm Petri dishes at a density of 0.5×10^6 cells per millilitre in RPMI 1640 medium containing 10% FBS, 10 IU/mL penicillin and 10 μg/mL streptomycin, and the cells were maintained at 37°C in a humidified atmosphere containing 5% CO_2. The THP-1 cells were differentiated into macrophages by the addition of 100 ng/mL PMA for 72 hours. For the immunocytochemistry experiment, THP-1 cells were seeded onto cover-slips in 35 mm Petri dishes. Macrophages were transformed into foam cells (FC) by incubation for 48 hours with 50 μg/mL ox-LDL (Union-Biology Co., Ltd, Beijing, China) in serum-free RPMI 1640 medium containing 0.3% BSA.

Accumulation of ALA-PpIX in sub-cellular organelles

To investigate the intracellular kinetics of ALA-PpIX, FCs were washed twice with phosphate-buffered saline (PBS) and incubated in the dark with 1.0 mM ALA (Sigma-Aldrich, St Louis, MO, USA) in serum-free medium at 37°C for different time intervals. FCs were then washed twice with PBS and fixed with 1% paraformaldehyde. The fluorescence of ALA-PpIX in FCs, mitochondria and ER was triggered by a violet light with a nominal operating wavelength of 405 nm and a line width of 20 nm, and the resulting fluorescence spectra were detected by an 8 nm resolution spectrometer [25]. Mitochondria and ER of FCs were isolated according to the manufacturers' instructions using a Mitochondria Isolation Kit and Endoplasmic Reticulum Isolation Kit (Sigma-Aldrich) separately.

Sub-cellular localisation of ALA-PpIX

After incubation with ALA, FCs were co-stained with 200 nM Mito-tracker green (Beyotime Biotechnology, Inc., Beijing, China) or 1 μM ER-TrackerTM Green (Molecular Probes, Carlsbad, CA, USA) for 30 minutes and 1 μg/mL 4',6-diamidine-2'-phenylindole dihydrochloride (DAPI) (F. Hoffmann-La Roche, Ltd, Basel, Switzerland) for 15 minutes in the dark at 37°C. Afterwards, FCs were observed under a laser scanning confocal microscope (LSCM, Model TCS SP5, Leica, Germany) to determine the sub-cellular localisation of ALA-PpIX. Fluorescence images were taken at the excitation/emission wavelengths of 405/610 nm for PpIX, 490/516 nm for Mito-tracker green, 504/511 nm for ER-TrackerTM Green and 360/460 nm for DAPI.

Sonication apparatus and treatment protocol

The ultrasonic generator, transducer and power amplifier were designed and assembled by the Harbin Institute of Technology (Harbin, China). A Petri dish was placed in a water bath at a 30 cm vertical distance above the ultrasonic transducer (diameter of 3.5 cm; resonance frequency of 1.0 MHz; duty factor of 10%; and repetition frequency of 100 Hz). The water in the glass tank was degassed beforehand [24].

FCs were divided into four groups as follows: control (Control), ALA alone (ALA), ultrasound alone (Ultrasound) and ultrasound plus ALA (SDT). FCs were incubated in the dark with 1.0 mM ALA for 2, 4, 6 and 8 hours at 37°C. In our previous study, THP-1 macrophages were treated with 0.5 W/cm^2 ultrasound [24]. Because foam cells are more sensitive to proapoptotic factors than normal macrophages, [26] ultrasound treatments of 0.3, 0.4 and 0.5 W/cm^2 for 5 minutes were applied. The temperature of the water was maintained at 25 ± 2°C during the sonication.

To study the roles of ROS, the mitochondria-caspase pathway and ER stress on the effects induced by ALA-SDT, a fraction of FCs was pretreated with 5 mM N-acetylcysteine (NAC; a ROS scavenger) (Sigma-Aldrich), 10 μM Z-VAD-FMK (pan-caspase inhibitor; Beyotime Biotechnology, Inc.) or 1 mM 4-phenylbutyrate (4-PBA; ER stress inhibitor) (Sigma-Aldrich) for 1 hour prior to the ultrasound exposure.

Cell apoptosis and necrosis assessment

After the sonication, FC apoptosis and necrosis were assessed by the Annexin V-PI apoptosis kit (BioseaBiotechnology Co., Ltd, Beijing, China) according to the manufacturer's instructions at 1, 2, 3, 4, 5 and 6 hours following the sonication. Hoechst 33342 (5 μg/mL; Molecular Probes) was added for 5 minutes before the endpoints of ALA-SDT treatment. The foam cells were then examined under an OLYMPUS IX81 fluorescence microscope, and images of 10-12 representative fields under green, red and blue fluorescence for Annexin V, PI and Hoechst 33342, respectively, were captured. Images were subsequently processed

using Image-Pro Plus software (Media Cybernetics, USA). Cell counting was performed based on the following protocol: apoptotic cells were stained with green fluorescence only (Annexin V^+/PI^-) and necrotic cells were stained with both green and red fluorescence or only red fluorescence (Annexin $V^{+/-}/PI^+$). The green apoptotic bodies are typically >3 μm structures. A net count of the total number of cells in the blue fluorescence field was performed. For statistical significance, more than 1000 total cells per group were counted, and each assessment was performed in triplicate. Treatment parameters that induced the highest apoptotic rate were used in the following experiments.

ROS assessment

Intracellular ROS levels were measured by staining with CellROX® Green Reagent (Molecular Probes). CellROX® Green Reagent (5 μM) was added to the FC medium for 30 minutes at 37°C after the sonication. After the FCs were washed three times with PBS, they were fixed with 3.7% formaldehyde for 15 minutes, and the cells were then examined under the fluorescence microscope. Fluorescence images were taken at the excitation/emission wavelengths of 488/520 nm. The levels of intracellular ROS were determined by the fluorescent intensity quantified with IOD values by Image-Pro Plus software. For statistical significance, more than 1000 total cells per group were counted, and the assessment was performed in triplicate.

Mitochondrial membrane potential (ΔΨm) detection

Mitochondrial membrane potential (Δψm) was assessed using the jc-1 fluorescent probe (Beyotime Biotechnology, Inc.). Immediately after sonication, cells were incubated in the dark with 10 mg/mL jc-1 for 20 minutes at 37°C and were assessed by the fluorescence microscope. Red–orange fluorescence can be attributed to a potential-dependent aggregation in the mitochondria. Green fluorescence, which reflects the monomeric form of jc-1, appeared in the cytosol after mitochondrial membrane depolarisation. The fluorescence intensity was measured using a fluorospectrophotometer (Varian Australia Pty Ltd, Melbourne, Victoria, Australia) with an excitation wavelength of 488 nm and emission wavelengths of 530 (green) and 590 nm (red). Each assessment was performed in triplicate.

Immunocytochemical staining

To detect cytochrome c translocation, FCs pretreated with 100 nM MitoTracker Deep Red FM (Molecular Probes) for 30 minutes were fixed with 1% paraformaldehyde for 15 minutes at 1 to 6 hours after the sonication. FCs were blocked with 1% BSA at room temperature for 20 minutes. Goat polyclone anti-cytochrome c primary antibody (1:250; Santa Cruz Biotechnology, Inc., CA, USA) was added to the Petri dishes at 4°C overnight. Rabbit anti-goat IgG Alexa Fluor 488 secondary antibody was then added for 1 hour followed by the addition of DAPI for 15 minutes at 37°C in the dark. After the staining, FCs were inverted on a microscope slide and observed under LSCM. The images showing MitoTracker Deep Red, Alexa Fluor 488 and DAPI fluorescence spectra were collected using 568, 488 and 360 nm excitation light, respectively.

Immunoblotting

SDS–PAGE and immunoblotting were performed as previously described [27]. Briefly, for the whole cell proteins, the proteins were obtained by centrifugation at 13000 rpm for 15 minutes at 4°C after being lysed in RIPA buffer (Beyotime Biotechnology, Inc.) on ice. For mitochondria and cytosolic proteins, mitochondria and cytosolic fractions were isolated using the Cell Mitochondria Isolation Kit (Beyotime Biotechnology, Inc.) according to the manufacturer's instructions for cytochrome c and BAX analyses. Protein concentrations were determined using a BCA Protein Assay Kit (Beyotime Biotechnology, Inc.). Protein samples were mixed with 5X SDS Loading buffer and separated by 10% SDS-PAGE. The proteins were then transferred onto nitrocellulose membranes and incubated overnight at 4°C with cytochrome c (1:500), rabbit anti-cleaved caspase 3 (1:1000; Cell Signaling Technology, Beverly, MA,USA), rabbit anti-cleaved caspase 9 (1:1000; Cell Signaling Technology), rabbit anti-Bcl-2 (1:1000; Cell Signaling Technology), mouse anti-Bax (1:1000; Santa Cruz Biotechnology, Inc.) and rabbit anti-GADD153 or C/EBP-homologous protein (CHOP) (1:1000; Santa Cruz Biotechnology, Inc.) primary antibodies with β-actin as the cytosolic loading control and COXIV as the mitochondria loading control. After washing three times with TBS-T, the membranes were incubated with secondary IgG antibodies linked to horseradish peroxidase, and protein levels were detected using an ECL detection system (Amersham Pharmacia Biotech, Uppsala, Sweden).

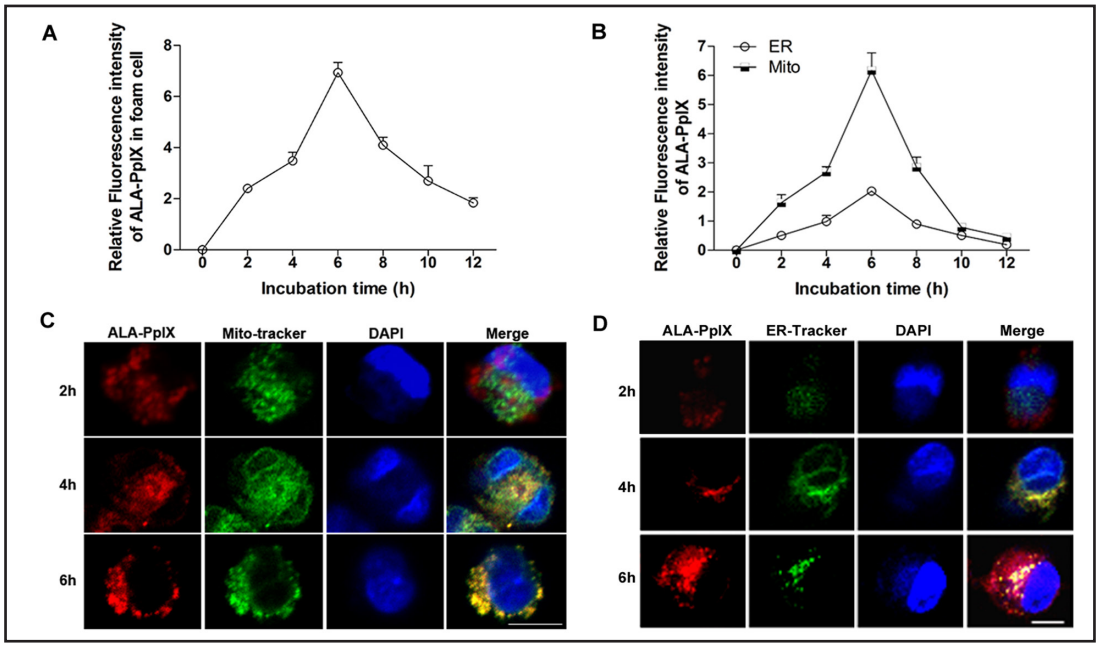

Fig. 1. Accumulation of intracellular ALA-PpIX and sub-cellular localisation of ALA-PpIX. The fluorescence intensity of ALA-PpIX in foam cells (A), and the extracted mitochondria and ER of foam cells (B) incubated with ALA for 0 to 12 hours. The fluorescence intensity peaked at 6 hours in the foam cells as well as in extracted mitochondria and ER detected by the spectrometer. The intensity in mitochondria was 3-fold higher than that in the ER at 6 hours. Representative LSCM images of sub-cellular localisation of ALA-PpIX in extracted mitochondria (C) and ER (D). Foam cells were subjected to green mito-tracker or ER tracker (green panel) and DAPI (blue panel) double staining following 2, 4 and 6 hour incubations with ALA. At 2 hours, ALA-PpIX (red panel) diffused in the cytoplasm showing a different pattern from that of the green mito-tracker or ER tracker and DAPI. At 4 hours, ALA-PpIX partially co-localised with the green mito-tracker or ER tracker. The yellow area represented the co-localisation of ALA-PpIX and the green mito-tracker or ER tracker. At 6 hours, ALA-PpIX was almost completely co-localised with the green mito-tracker, but inclusion of the ER tracker. The red fluorescence intensity increased with time. Note: Scale bar = 10 μm.

Statistical analysis

All data are shown as the mean value ± standard deviation (SD). The difference among groups was analysed according to one-way analysis of variance followed by Student–Newman–Keuls tests. Statistical evaluation was performed using SPSS 13.0 software. Differences were considered statistically significant when $P<0.05$.

Results

Accumulation of intracellular and mitochondrial ALA-PpIX and sub-cellular localisation of ALA-PpIX

As shown in Fig. 1A and 1B, the fluorescence intensity of ALA-PpIX detected by the spectrometer was increased with time and peaked at 6 hours in the foam cells as well as in extracted mitochondria and ER, and the fluorescence then faded with time. The fluorescence intensity in mitochondria was 3-fold higher than that in the ER at 6 hours.

The sub-cellular location patterns of ALA-PpIX are shown in Fig. 1C and 1D. ALA-PpIX was detected mainly in the cytoplasm 2 hours after adding ALA showing a different pattern from that of the green mito-tracker or ER tracker. With the lapse of time, ALA-PpIX began to partially co-localise with the green mito-tracker or ER tracker at 4 hours of incubation, and it almost completely co-localised with the green mito-tracker, but inclusion of the ER tracker, at 6 hours of incubation. Furthermore, the fluorescence intensity of ALA-PpIX in the foam cells increased gradually with time within 6 hours, which was consistent with the results of

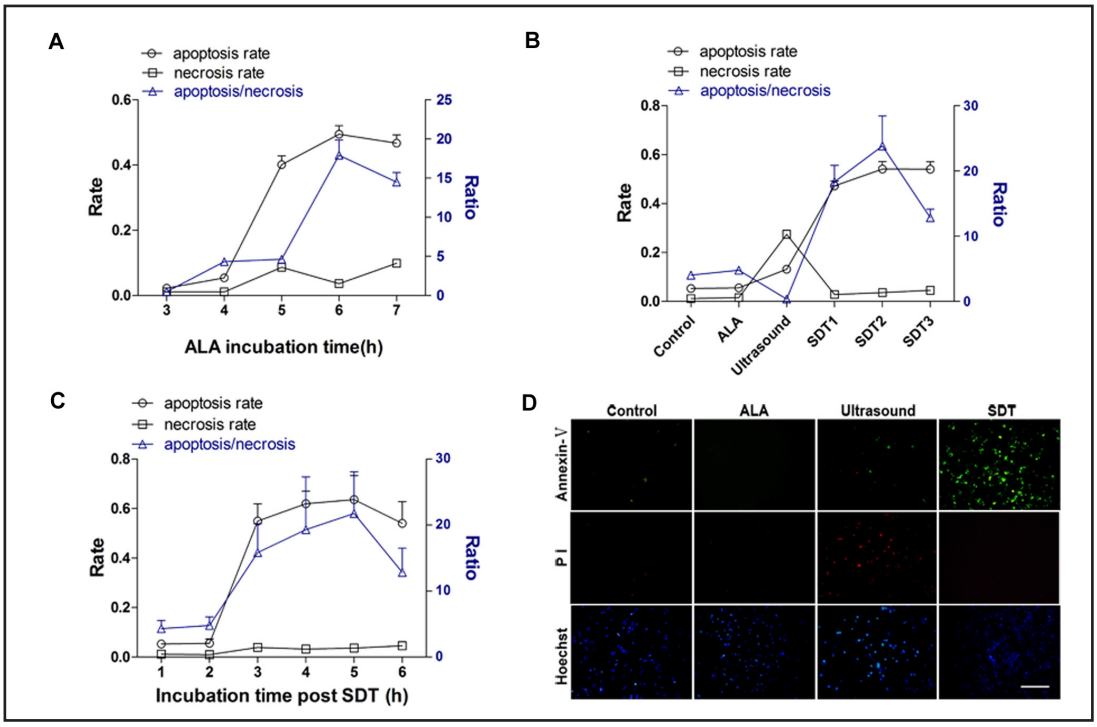

Fig. 2. Apoptosis induction with ALA-SDT. The apoptotic rate, necrotic rate and apoptosis/necrosis ratio of foam cells (A) with different ALA incubation times and 0.4 W/cm^2 ultrasonic irradiation as determined by the Annexin V-PI assay. (B) The apoptotic rate, necrotic rate and apoptosis/necrosis ratio of foam cells in the Control, ALA, Ultrasound (0.4 W/cm^2), SDT1 (0.3 W/cm^2 ultrasound plus ALA), SDT2 (0.4 W/cm^2 ultrasound plus ALA) and SDT3 (0.5 W/cm^2 ultrasound plus ALA) groups with a 6 hour ALA incubation time as determined by the Annexin V-PI assay. (C) The apoptotic rate, necrotic rate and apoptosis/necrosis ratio of foam cells with different incubation times after ALA-SDT (6 hour ALA incubation time plus 0.4 W/cm^2 ultrasonic irradiation) as determined by the Annexin V-PI assay. Data are presented as the mean ± SD values. More than 1000 total cells per group were counted, and the assessment was performed in triplicate. (D) Fluorescent micrographs of foam cells in the Control, ALA (6 hour incubation), Ultrasound (0.4 W/cm^2) and SDT (6 hour ALA incubation plus 0.4 W/cm^2 ultrasonic irradiation) groups stained with Annexin V-PI and Hoechst 33342 5 hours after the treatment. Note: Scale bar = 0.2 mm.

the spectrometric measurements.

Apoptosis of THP-1 macrophage-derived foam cells induced by ALA-SDT

To optimise the treatment conditions and induce the highest rate of apoptosis, cell apoptosis and necrosis were assessed by the Annexin V-PI apoptosis kit according to the manufacturer's instructions. As shown in Fig. 2A, at 6 hours after the 0.4 W/cm^2 ultrasonic irradiation, the percentage of apoptotic cells increased significantly from the 2 hour ALA incubation time (2.3 ± 1.2%) to the 6 hour incubation time (49.5 ± 6.7%). The maximum apoptosis/necrosis ratio (17.9 ± 5.5) was observed at the 6 hour ALA incubation time, while the necrosis rate was slightly increased from the 2 hour (1.1 ± 0.4%) to 6 hour ALA incubation time (3.7 ± 1.6%). As shown in Fig. 2B, using a 6 hour incubation time with ALA, the percentage of apoptotic cells increased significantly in the SDT groups (47.3 ± 5.5%, 54.2 ± 9.5% and 53.8 ± 8.8% for 0.3, 0.4 and 0.5 W/cm^2, respectively) compared to the Control, ALA and Ultrasound groups (5.3 ± 1.1%, 5.5 ± 1.7% and 13.2 ± 3.2%, respectively). The maximum ratio of apoptosis/necrosis was observed in the 0.4 W/cm^2 SDT group (28.8 ± 12.1). As shown in Fig. 2C, for the group incubated with ALA for 6 hours and irradiated with 0.4 W/cm^2 sonication, the percentage of apoptotic cells increased with time after the treatment and reached a peak at 5 hours (63.6 ± 9.8%), which was the same as the apoptosis/necrosis ratio

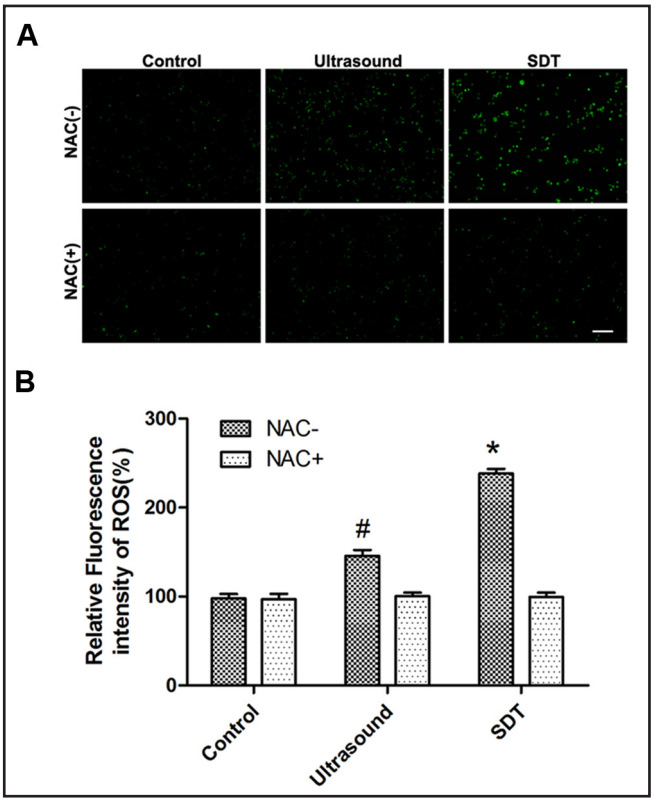

Fig. 3. Intracellular ROS formation in foam cells induced by ALA-SDT. (A) Fluorescent micrographs of foam cells showing intracellular ROS formation as stained by the CellROX® Green Reagent. Light green fluorescence indicates increased levels of ROS in the cytoplasm of the foam cells immediately after SDT, which was inhibited by the ROS scavenger, NAC. (B) Levels of intracellular ROS determined by the fluorescent intensity quantified with IOD values. Data are presented as the mean ± SD values. More than 1000 total cells per group were counted, and the assessment was performed in triplicate. **P*<0.01 versus Control, Ultrasound, SDT plus NAC groups; #*P*<0.01 versus Control, Ultrasound plus NAC groups. Note: Scale bar = 0.2 mm.

(peaked at 21.7 ± 6.3 at 5 hours). The fluorescent images of the four groups of the foam cells 5 hours after the treatment are shown in Fig. 2D. Therefore, a 6 hour incubation time with ALA and ultrasonic intensity of 0.4 W/cm^2 were used in the following experiments.

ROS production induced by ALA-SDT

Previous studies have shown that SDT can increase the level of intracellular ROS in tumour cells *in vitro*, [9-12] so we monitored intracellular ROS formation by staining with the CellROX® Green Reagent. As shown in Fig. 3A and 3B, compared with the Control group (98.2 ± 10.5%), green fluorescence increased significantly in the Ultrasound group (145.8 ± 14.4%; *P*<0.01 vs. Control group) and SDT group (238.4 ± 11.7%; *P*<0.01 vs. Control and Ultrasound groups) immediately after the treatment, and this fluorescence was inhibited by adding the ROS scavenger, NAC (99.6 ± 10.7%; *P*<0.01 vs. SDT group).

Collapse of mitochondrial membrane potential (ΔΨm) induced by ALA-SDT

As shown in Fig. 4A, the green and red-orange fluorescence microscopic images of jc-1 were captured to evaluate SDT-induced changes of membrane potential (Δψm). As shown in Fig. 4B, compared with Control group (100.0 ± 3.0%), the Δψm in the Ultrasound group was significantly decreased (71.9 ± 6.0%; *P*<0.05 vs. Control group), and the Δψm in the SDT group was even further decreased (2.3 ± 0.9%; *P*<0.01 vs. Control group), thereby indicating that the sensitivity of mitochondria to sonication was significantly enhanced by ALA-PpIX. By adding the ROS scavenger, NAC, the Δψm showed no obvious changes in the Ultrasound group, but the Δψm decrease was significantly inhibited in the SDT group (32.7 ± 13.3%; *P*<0.01 vs. SDT group).

Mitochondria-caspase pathway activated by ALA-SDT

As shown in Fig. 5A, at 5 hours after ALA-SDT treatment, a diffused green fluorescence was observed indicating the translocation of cytochrome c from mitochondria to the cytosol, but cytochrome c was closely anchored to the mitochondria in the Control group and NAC-

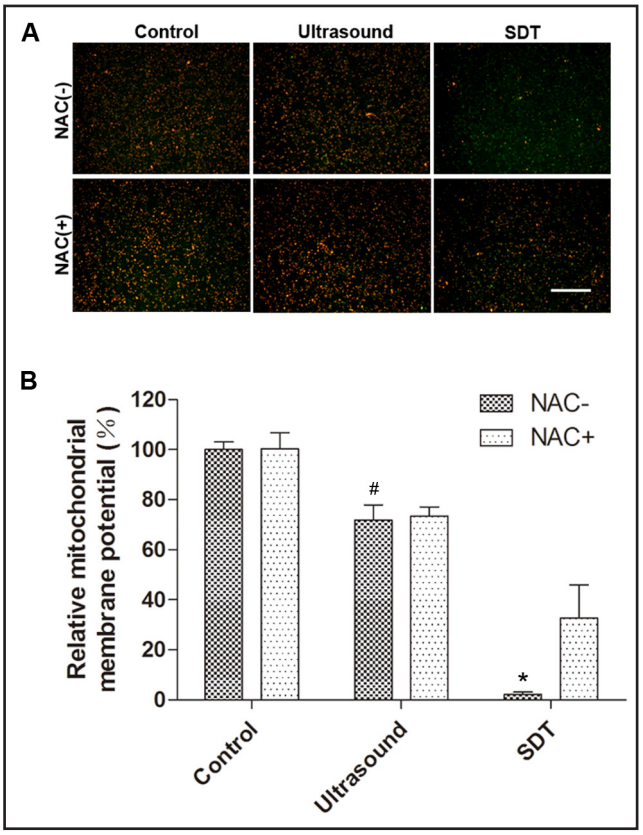

Fig. 4. Alteration of mitochondrial membrane potential induced by ALA-SDT. (A) Fluorescent micrographs of foam cells stained with jc-1 immediately after treatment. Mitochondrial membrane potential collapse was observed in the SDT group, which was inhibited by the pretreatment of NAC. (B) The relative mitochondrial membrane potential levels of foam cells as assessed by a fluorospectrophotometer. Data are presented as the mean ± SD values (n = 6 per group). Each assessment was performed in triplicate. **P*<0.01 versus Control, Ultrasound, SDT plus NAC groups; #*P*<0.05 versus Control group. Note: Scale bar = 1.0 mm.

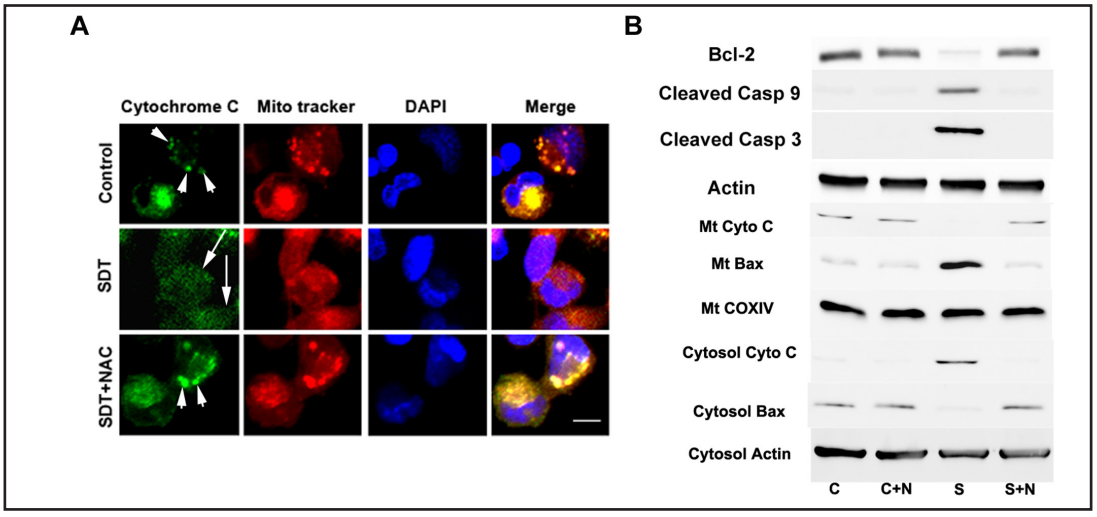

Fig. 5. Activation of the mitochondrial pathway of apoptosis by ALA-SDT. (A) Representative LSCM images of the translocation of cytochrome c induced by ALA-SDT. Foam cells were pretreated with 100 nM MitoTracker Deep Red FM (red panel), incubated with anti-cytochrome c primary antibody and labelled with Alexa Fluor 488 secondary antibody (green panel) and DAPI (blue panel). Five hours after SDT, cytochrome c diffused in the cytosol (long arrow). In the Control and NAC-pretreated SDT groups, cytochrome c was closely anchored to the mitochondria (short arrows). (B) Activation of mitochondrial pathway-associated proteins by ALA-SDT as analysed by immunoblotting, and the induction of these proteins was inhibited by the ROS scavenger, NAC. Note: Scale bar = 10 μm.

pretreated ALA-SDT group. This result was consistent with the translocation of cytochrome c from mitochondria into the cytosol in the SDT group as analysed by western blot (Fig. 5B). Moreover, translocation of BAX (mitochondria proapoptotic regulatory factor) from the

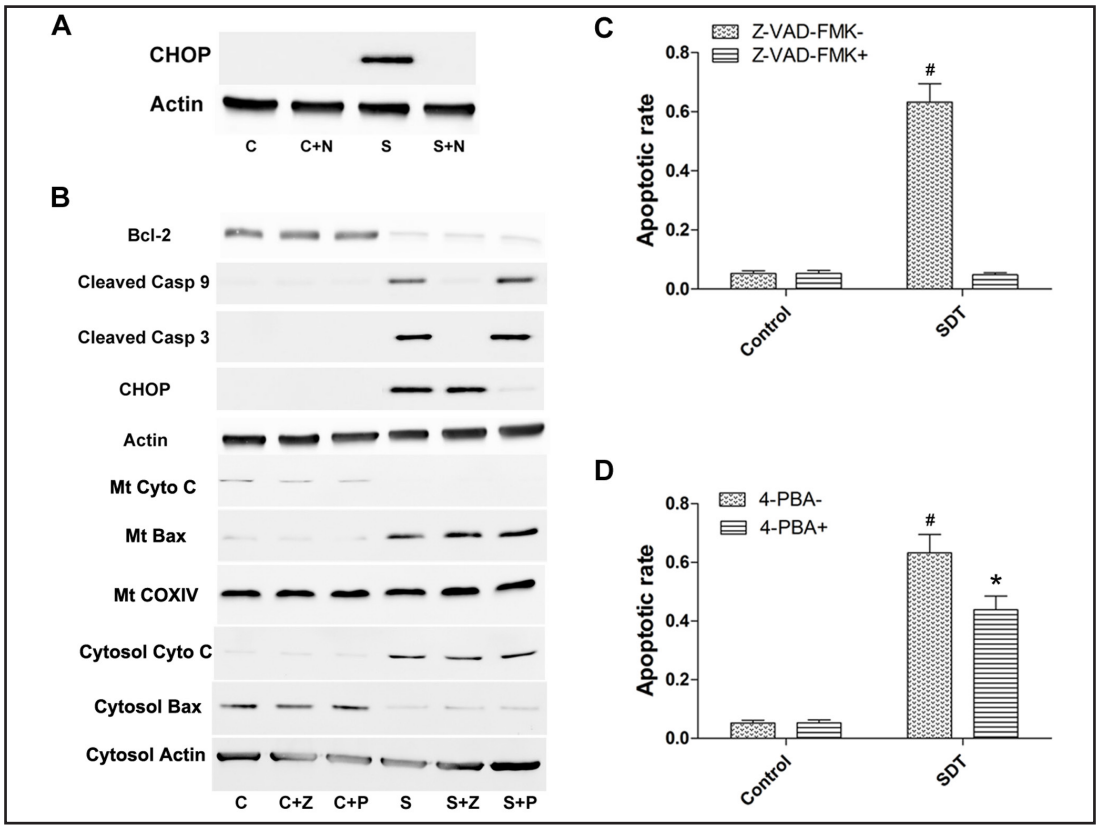

Fig. 6. The mitochondria-caspase pathway was the predominant pathway in apoptosis induced by ALA-SDT although ER stress was induced. (A) Activation of the ER stress-associated protein, CHOP, by ALA-SDT, and this induction was inhibited by the ROS inhibitor, NAC. (B) Effects of Z-VAD-FMK and 4-PBA on the activation of the mitochondrial pathway and ER stress induced by ALA-SDT. Effects of Z-VAD-FMK (C) and 4-PBA (D) on ALA-SDT-induced foam cell apoptosis as determined by the Annexin V-PI assay. Data are presented as the mean ± SD values. More than 1000 total cells per group were counted, and the assessment was performed in triplicate. #P<0.01 versus Control group, SDT plus Z-VAD-FMK group or SDT plus 4-PBA group. *P<0.01 versus Control group.

cytosol to mitochondria, cleavage of active caspase 9 (apoptotic initiator factor), cleavage of active caspase 3 (executive factor) and downregulation of Bcl-2 (mitochondria antiapoptotic regulatory factor) were detected in the SDT group compared to the Control group, which was inhibited by the pretreatment of NAC.

ER stress participates in ALA-SDT-induced apoptosis but the mitochondria-caspase pathway is predominant

As shown in Fig. 6A, an upregulation of CHOP was detected in the SDT group, which was inhibited by NAC pretreatment, thereby indicating that ROS played a key role in the induction of ER stress under ALA-SDT treatment. As shown in Fig. 6B, the upregulation of CHOP was inhibited significantly in the 4-PBA pretreatment ALA-SDT group, but there were no obvious changes in the mitochondrial pathway apoptosis-associated factors. In contrast, pretreatment with the pan-caspase inhibitor, Z-VAD-FMK, inhibited the cleavage of caspase 3 and caspase 9, but pretreatment with Z-VAD-FMK did not inhibit the translocations of cytochrome c and BAX or the changes of Bcl-2 and CHOP. As shown in Fig. 6C, compared with the SDT group (63.3 ± 6.2%), Z-VAD-FMK significantly reduced apoptosis induced by ALA-SDT (4.8 ± 0.7%; P<0.01 vs. SDT group), which was similar to that of the Control group (4.5 ± 0.6%), and 4-PBA only reduced apoptosis by one-third as shown in Fig. 6D (43.8 ± 4.7%; P<0.01 vs. SDT group).

Discussion

This study reported the following results: 1) the majority of ALA-PpIX accumulates in mitochondria and the ER of FCs at 6 hours of ALA administration, and the fluorescence intensity in mitochondria is 3-fold higher than that in the ER; 2) the highest apoptotic rate can be achieved when FCs are exposed to ultrasound 6 hours after ALA administration; 3) the mitochondria-caspase pathway and ER stress can be activated simultaneously by ROS derived from ALA-SDT; and 4) the mitochondria-caspase pathway is the predominant pathway in ALA-SDT-induced apoptosis despite the presence of ER stress.

Considering the ALA-derived sonosensitiser, PpIX, is synthesised in the mitochondria intermembrane space, [14-16] the time point at which the highest accumulation of ALA-PpIX in the mitochondria occurs may be the best time to induce a burst of apoptosis by ALA-SDT. We examined the pharmacokinetics and sub-cellular location of ALA-PpIX in FCs. We showed that the time for peak intracellular ALA-PpIX concentrations in the whole cell, extracted mitochondria and ER was 6 hours, and we also showed that the intensity of ALA-PpIX fluorescence in mitochondria was 3-fold higher than that in the ER (Fig.s 1A and 1B). Our previous study demonstrated that the intracellular ALA-PpIX levels reach a peak level at 3 hours in THP-1 macrophages [24]. The difference of the peak time between the THP-1 macrophages and FCs may suggest a low metabolic rate in foam cells. X.B. Wang et al. studied the pharmacokinetics of ALA-PpIX in sarcoma 180 cells and found that ALA-PpIX accumulates in a time-dependent manner up to 12 hours of incubation without a peak concentration level [14]. Kuzelová et al. observed a plateau in K562 cells at 4 to 8 hours of incubation [28]. These differences suggest that different cell lines have different metabolic features. Consistent with the pharmacokinetics results, we observed by LSMC that ALA-PpIX mainly accumulated in the cytosol after 2 hours of ALA incubation (Fig. 1C), and there was no obvious apoptosis or necrosis detected despite the presence of sonication at this time (Fig. 2A). The result was in accordance with that of X.B. Wang et al., who found no effect of SDT when exo-PpIX was localised in the cytosol of S180 cells [14]. When FCs were sonicated after 6 hours of ALA incubation, the expected burst of the apoptotic rate (63.6 ± 9.8%) occurred without obvious necrosis (Fig. 2C). For THP-1 macrophages, in contrast, ALA-SDT induces 25.3 ± 3.0% apoptosis, and emodin-SDT induces 32 ± 6% apoptosis [24, 29]. This much higher level of apoptosis achieved in FCs might be due to the exact sub-cellular location of ALA-PpIX in the mitochondria and the ALA-PpIX metabolic feature in FCs.

Studies have reported mitochondrial damage in tumour cells induced by SDT [15, 30]. It has been widely accepted that the mechanism of SDT inducing cellular damage is the formation of ROS triggered by the activation of the sonosensitiser in the binding site [10, 12, 16, 30]. Mitochondrial lipid peroxidation products contributing to the generation of ROS can impair the barrier function of membranes by either directly interacting with the protein and/or indirectly interacting with the lipid moieties in the membrane, thus leading to mitochondrial outer membrane permeabilisation and activation of an intrinsic mitochondria apoptotic pathway [31]. In this study, we detected ROS formation (Fig.s 3A and 3B) and $\Delta\psi m$ collapse immediately after ALA-SDT (Fig.s 4A and 4B), and the latter was partially inhibited by the ROS scavenger, NAC, thereby indicating that ROS generation plays a role in altering mitochondria function induced by ALA-SDT. Cytochrome c is released from the intermembrane space of mitochondria into the cytoplasm and subsequently associates with procaspase-9/Apaf 1, which activates effector caspases 9 and 3 to initiate the caspase cascade, thus inducing cellular apoptosis [23, 31-33]. In accordance with this theory, we detected the translocation of cytochrome c from mitochondria into the cytoplasm (Fig.s 5A and 5B) and activation of both caspases 9 and 3 5 hours after ALA-SDT (Fig. 5B), thereby indicating that the mitochondria-caspase pathway is involved in apoptosis induced by ALA-SDT. We also found that the pro-apoptotic factor, BAX, and the anti-apoptotic factor, Bcl-2, participated in the apoptotic event (Fig. 5B). BAX and Bcl-2 are members of the Bcl-2 family that directly regulate and mediate mitochondrial outer membrane permeabilisation [23, 33]. The mitochondria-caspase apoptotic pathway induced by ALA-SDT was inhibited by the

ROS scavenger, NAC (Fig. 5B). Thus, ROS derived from ALA-PpIX may be the main effector that caused the mitochondrial damage.

In addition to mitochondria, ER stress can also initiate apoptosis through activating three branches of the unfolded protein response (UPR), including IRE1α, ATF6 and PERK pathways [3, 6, 34]. CHOP, as a transcriptional target of PERK, IRE1α–XBP-1 and ATF6, links the three branches of the UPR [6]. Chronic ER stress can induce widespread pathologic apoptosis [6]. Studies have established the role of CHOP in ER stress-induced foam cell apoptosis in advanced atherosclerosis [6, 34]. Foam cells that undergo chronic ER stress secret inflammatory cytokines, and the apoptosis triggered by chronic ER stress elicits an inflammatory response in phagocytes [7, 35]. Because ALA-PpIX was also distributed in the ER of FCs (although the fluorescence intensity was one-third of that in mitochondria), we evaluated the ER stress by determining CHOP expression after FCs were subjected to ALA-SDT. The upregulation of CHOP in the SDT group verified the occurrence of ER stress (Fig. 6A). To evaluate the dominant pathway mediating apoptosis between ER stress and mitochondria stress in FC apoptosis induced by ALA-SDT, we pretreated FCs with the ER stress inhibitor, 4-PBA, and the pan-caspase inhibitor, Z-VAD-FMK. The results showed that 4-PBA inhibited CHOP expression and blocked one-third of the apoptosis, but 4-PPBA did not inhibit the initiation of the mitochondria-caspase pathway. Moreover, Z-VAD-FMK inhibited the activity of caspase 9 and caspase 3 as well as blocked all of the apoptosis induced by ALA-SDT, but Z-VAD-FMK did not block CHOP expression (Fig.s 6B, 6C and 6D). These results indicated that initiation of ER stress and the mitochondria-caspase pathway were parallel and independent of each other, and these results also demonstrated that the mitochondria-caspase pathway was the predominant pathway in the apoptosis induced by ALA-SDT although ER stress was induced.

In conclusion, our results demonstrated that ALA-SDT simultaneously activated the mitochondria-caspase pathway and ER stress in THP-1 macrophage-derived foam cells and that ROS was the main effector. The mitochondria-caspase pathway was the predominant pathway in the ALA-SDT-induced apoptosis although ER stress was induced. Our findings may provide evidence for targeted atherosclerosis therapy by ALA-SDT. In the future, we plan to conduct more *in vivo* experiments in atherosclerotic plaques and to provide additional evidence for this non-invasive approach to treat atherosclerosis.

Acknowledgments

This study was supported by the National Natural Science Foundation of China (81171483, 81371709), the Postgraduate Creative Research Foundation of Heilongjiang Province, China (YJSCX2011-329HLJ) and the Scientific Research Foundation of the Health Bureau of Heilongjiang Province, China (2012-579). This study was also supported by grants from the Funds for Creative Research Groups of the National Natural Science Foundation of China (81121003).

Disclosure Statement

None declared.

References

1 Capewell S, Lloyd-Jones DM: Optimal cardiovascular prevention strategies for the 21st century. JAMA 2010;304:2057-2058.

2 Roger VL, Go AS, Lloyd-Jones DM, Benjamin EJ, Berry JD, Borden WB, Bravata DM, Dai S, Ford ES, Fox CS, Fullerton HJ, Gillespie C, Hailpern SM, Heit JA, Howard VJ, Kissela BM, Kittner SJ, Lackland DT, Lichtman JH, Lisabeth LD, Makuc DM, Marcus GM, Marelli A, Matchar DB, Moy CS, Mozaffarian D, Mussolino ME, Nichol G, Paynter NP, Soliman EZ, Sorlie PD, Sotoodehnia N, Turan TN, Virani SS, Wong ND, Woo D, Turner MB; American Heart Association Statistics Committee and Stroke Statistics Subcommittee: Heart disease and stroke statistics--2012 update: a report from the American Heart Association. Circulation 2012;125:e2-e220.
3 Moore KJ, Tabas I: Macrophages in the pathogenesis of atherosclerosis. Cell 2011;145:341-355.
4 Tabas I, Williams KJ, Boren J: Subendothelial lipoprotein retention as the initiating process in atherosclerosis: update and therapeutic implications. Circulation 2007;116:1832-1844.
5 Tabas I: Macrophage death and defective inflammation resolution in atherosclerosis. Nat Rev Immunol 2010;10:36-46.
6 Tabas I, Ron D: Integrating the mechanisms of apoptosis induced by endoplasmic reticulum stress. Nat Cell Biol 2011;13:184-190.
7 Li Y, Schwabe RF, DeVries-Seimon T, Yao PM, Gerbod-Giannone MC, Tall AR, Davis RJ, Flavell R, Brenner DA, Tabas I: Free cholesterol-loaded macrophages are an abundant source of tumor necrosis factor-alpha and interleukin-6: model of NF-kappaB- and map kinase-dependent inflammation in advanced atherosclerosis. J Biol Chem 2005;280:21763-21772.
8 Yumita N, Nishigaki R, Umemura K, Umemura S: Hematoporphyrin as a sensitizer of cell-damaging effect of ultrasound. Jpn J Cancer Res 1989;80:219-222.
9 Rosenthal I, Sostaric JZ, Riesz P: Sonodynamic therapy--a review of the synergistic effects of drugs and ultrasound. Ultrason Sonochem 2004;11:349-363.
10 Tang W, Liu Q, Wang X, Wang P, Zhang J, Cao B: Potential mechanism in sonodynamic therapy and focused ultrasound induced apoptosis in sarcoma 180 cells in vitro. Ultrasonics 2009;49:786-793.
11 Song W, Cui H, Zhang R, Zheng J, Cao W: Apoptosis of SAS cells induced by sonodynamic therapy using 5-aminolevulinic acid sonosensitizer. Anticancer Res 2011;31:39-45.
12 Tsuru H, Shibaguchi H, Kuroki M, Yamashita Y: Tumor growth inhibition by sonodynamic therapy using a novel sonosensitizer. Free Radic Biol Med 2012;53:464-472.
13 Gao Z, Zheng J, Yang B, Wang Z, Fan H, Lv Y, Li H, Jia L, Cao W: Sonodynamic therapy inhibits angiogenesis and tumor growth in a xenograft mouse model. Cancer Lett 2013;335:93-99.
14 Wang X, Wang P, Tong W, Liu Q: Comparison of pharmacokinetics, intracellular localizations and sonodynamic efficacy of endogenous and exogenous protoporphyrin IX in sarcoma 180 cells. Ultrasonics 2010;50:803-810.
15 He Y, Xia X, Xu C, Yu H, Bai D, Xiang J, Leung AW: 5-Aminolaevulinic acid enhances ultrasound-induced mitochondrial damage in K562 cells. Ultrasonics 2010;50:777-781.
16 Lv Y, Fang M, Zheng J, Yang B, Li H, Xiuzigao Z, Song W, Chen Y, Cao W: Low-intensity ultrasound combined with 5-aminolevulinic acid administration in the treatment of human tongue squamous carcinoma. Cell Physiol Biochem 2012;30:321-333.
17 Yumita N, Umemura S, Magario N, Umemura K, Nishigaki R: Membrane lipid peroxidation as a mechanism of sonodynamically induced erythrocyte lysis. Int J Radiat Biol 1996;69:397-404.
18 Kinoshita M, Hynynen K: Mechanism of porphyrin-induced sonodynamic effect: possible role of hyperthermia. Radiat Res 2006;165:299-306.
19 Mi N, Liu Q, Wang X, Zhao X, Tang W, Wang P, Cao B: Induction of sonodynamic effect with protoporphyrin IX on isolate hepatoma-22 cells. Ultrasound Med Biol 2009;35:680-686.
20 Danial NN, Korsmeyer SJ: Cell death: critical control points. Cell 2004;116:205-219.
21 Gogvadze V, Orrenius S, Zhivotovsky B: Mitochondria as targets for chemotherapy. Apoptosis 2009;14:624-640.
22 Savill J, Dransfield I, Gregory C, Haslett C: A blast from the past: clearance of apoptotic cells regulates immune responses. Nat Rev Immunol 2002;2:965-975.
23 Spierings D, McStay G, Saleh M, Bender C, Chipuk J, Maurer U, Green DR: Connected to death: the (unexpurgated) mitochondrial pathway of apoptosis. Science 2005;310:66-67.
24 Cheng J, Sun X, Guo S, Cao W, Chen H, Jin Y, Li B, Li Q, Wang H, Wang Z, Zhou Q, Wang P, Zhang Z, Cao W, Tian Y: Effects of 5-aminolevulinic acid-mediated sonodynamic therapy on macrophages. Int J Nanomedicine 2013;8:669-676.

25 Cheng J, Liang H, Li Q, Peng C, Li Z, Shi S, Yang L, Tian Z, Tian Y, Zhang Z, Cao W: Hematoporphyrin monomethyl ether-mediated photodynamic effects on THP-1 cell-derived macrophages. J Photochem Photobiol B 2010;101:9-15.
26 Tabas I: Free cholesterol-induced cytotoxicity a possible contributing factor to macrophage foam cell necrosis in advanced atherosclerotic lesions. Trends Cardiovasc Med 1997;7:256-263.
27 Liu X, Kim CN, Yang J, Jemmerson R, Wang X: Induction of apoptotic program in cell-free extracts: requirement for dATP and cytochrome c. Cell 1996;86:147-157.
28 Kuzelova K, Grebenova D, Pluskalova M, Marinov I, Hrkal Z: Early apoptotic features of K562 cell death induced by 5-aminolaevulinic acid-based photodynamic therapy. J Photochem Photobiol B 2004;73:67-78.
29 Gao Q, Wang F, Guo S, Li J, Zhu B, Cheng J, Jin Y, Li B, Wang H, Shi S, Gao Q, Zhang Z, Cao W, Tian Y: Sonodynamic effect of an anti-inflammatory agent--emodin on macrophages. Ultrasound Med Biol 2011;37:1478-1485.
30 30. Tang W, Liu Q, Zhang J, Cao B, Zhao P, Qin X: In vitro activation of mitochondria-caspase signaling pathway in sonodynamic therapy-induced apoptosis in sarcoma 180 cells. Ultrasonics 2010;50:567-576.
31 Gupta S, Kass GE, Szegezdi E, Joseph B: The mitochondrial death pathway: a promising therapeutic target in diseases. J Cell Mol Med 2009;13:1004-1033.
32 Susin SA, Lorenzo HK, Zamzami N, Marzo I, Snow BE, Brothers GM, Mangion J, Jacotot E, Costantini P, Loeffler M, Larochette N, Goodlett DR, Aebersold R, Siderovski DP, Penninger JM, Kroemer G: Molecular characterization of mitochondrial apoptosis-inducing factor. Nature 1999;397:441-446.
33 Green DR, Kroemer G: The pathophysiology of mitochondrial cell death. Science 2004;305:626-629.
34 Tabas I, Seimon T, Timmins J, Li G, Lim W: Macrophage apoptosis in advanced atherosclerosis. Ann N Y Acad Sci 2009;1173:S E40-45.
35 Li Y, Gerbod-Giannone MC, Seitz H, Cui D, Thorp E, Tall AR, Matsushima GK, Tabas I: Cholesterol-induced apoptotic macrophages elicit an inflammatory response in phagocytes, which is partially attenuated by the Mer receptor. J Biol Chem 2006;281:6707-6717.